

# UNCLASSIFIED

AD NUMBER
AD858522
NEW LIMITATION CHANGE
TO Approved for public release, distribution unlimited
FROM Distribution authorized to U.S. Gov't. agencies and their contractors; Critical Technology; 15 AUG 1969. Other requests shall be referred to Space and Missile Systems Organization, Los Angeles AFS, CA 90045.
AUTHORITY
SAMSO ltr dtd 19 Jan 1972

THIS PAGE IS UNCLASSIFIED

AD858522

## Reentry Plasma Attenuation for S-Band Telemetry Systems

Prepared by K. E. GOLDEN  
Plasma Research Laboratory

69 AUG 15

---

Laboratory Operations  
AEROSPACE CORPORATION

---

DDC  
RECEIVED  
SEP 15 1969  
RECEIVED  
B

Prepared for SPACE AND MISSILE SYSTEMS ORGANIZATION  
AIR FORCE SYSTEMS COMMAND  
LOS ANGELES AIR FORCE STATION  
Los Angeles, California



THIS DOCUMENT IS SUBJECT TO SPECIAL EXPORT  
CONTROLS AND EACH TRANSMITTAL TO FOREIGN  
GOVERNMENTS OR FOREIGN NATIONALS MAY BE MADE  
ONLY WITH PRIOR APPROVAL OF SAMSO (SMTAE).  
THE DISTRIBUTION OF THIS REPORT IS LIMITED BE-  
CAUSE IT CONTAINS TECHNOLOGY RESTRICTED BY  
MUTUAL SECURITY ACTS.

144

Air Force Report No.  
SAMSO-TR-69-242

Aerospace Report No.  
TR-0066(4220-10)-1  
(Formerly TR-0200(4220-10)-3)

REENTRY PLASMA ATTENUATION FOR  
S-BAND TELEMETRY SYSTEMS

Prepared by

K. E. Golden  
Plasma Research Laboratory

69 AUG 15

Laboratory Operations  
AEROSPACE CORPORATION

Prepared for

SPACE AND MISSILE SYSTEMS ORGANIZATION  
AIR FORCE SYSTEMS COMMAND  
LOS ANGELES AIR FORCE STATION  
Los Angeles, California

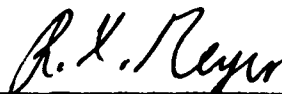
This document is subject to special export controls and each transmittal to foreign governments or foreign nationals may be made only with prior approval of SAMSO(SMTAE). The distribution of this report is limited because it contains technology restricted by mutual security acts.

## FOREWORD

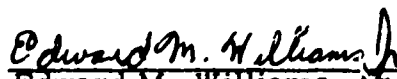
This document is published by The Aerospace Corporation,  
El Segundo, California, under Air Force Contract No. F04701-69-C-0066.

This report, which documents research carried out during January  
1969, was submitted on 19 June 1969 to Lieutenant Edward M. Williams, Jr.,  
SMTAE, for review and approval.

Approved

  
\_\_\_\_\_  
R. X. Meyer, Director  
Plasma Research Laboratory

Publication of this report does not constitute Air Force approval  
of the report's findings or conclusions. It is published only for the  
exchange and stimulation of ideas.

  
\_\_\_\_\_  
Edward M. Williams, Jr.  
2nd Lt., United States Air Force  
Project officer

## ABSTRACT

The performance of a slot telemetry antenna is analyzed, including the effects of an inhomogeneous plasma sheath on aperture admittance, radiation pattern distortion, antenna window absorption, reflection and absorption losses of the feed network, and total antenna gain. The change in broadside antenna gain induced by the reentry plasma sheath is compared with plane wave signal attenuation calculations. Various antenna matching conditions are evaluated for free-space and reentry-plasma conditions.

## CONTENTS

FOREWORD .....	ii
ABSTRACT .....	iii
I. INTRODUCTION .....	1
II. APERTURE ADMITTANCE .....	5
III. ANTENNA GAIN .....	9
IV. FEED NETWORK .....	13
V. NUMERICAL RESULTS .....	15
A. Aperture Admittance .....	15
B. Free Excitation Antenna Gain .....	18
C. Feed Calculations .....	18
D. Absorption Effects in the Waveguide Antenna Window .....	27
E. Matching to a Plasma Environment .....	33
IV. CONCLUSIONS .....	37
REFERENCES .....	39

## FIGURES

1.	Slot Geometry . . . . .	2
2.	Feed Network . . . . .	3
3.	Reentry Plasma Sheath . . . . .	16
4.	Aperture Admittance . . . . .	17
5.	E-Plane Antenna Gain . . . . .	19
6.	H-Plane Antenna Gain . . . . .	20
7.	Feed Network Insertion Loss . . . . .	22
8.	Reflection Loss vs Electron Density . . . . .	23
9.	Change in Antenna Gain with Aperture Matched to Free Space . . . . .	25
10.	Input VSWR with Aperture Matched to Free Space . . . . .	26
11.	Plane Wave Attenuation Error . . . . .	28
12.	Thin Sheath Limit for Change in Antenna Gain with Aperture Matched to Free Space . . . . .	29
13.	Thin Sheath Limit for Input VSWR with Aperture Matched to Free Space . . . . .	30
14.	Reduction in Antenna Gain Caused by by Window Absorption . . . . .	31
15.	Reflection Loss vs Window Absorption . . . . .	32
16.	Input Admittance for Various Matching Conditions . . . . .	34
17.	Change in Antenna Gain for Various Matching Conditions . . . . .	35
18.	Input VSWR for Various Matching Conditions . . . . .	36

## TABLES

1.	Physical Dimensions of Waveguide Window . . . . .	15
2.	Matching Conditions . . . . .	33

## I. INTRODUCTION

The antenna gain characteristics of a simple S-band telemetry antenna system radiating through an inhomogeneous plasma sheath have been analyzed. Aperture admittance, radiation pattern, signal attenuation, matching network, and resulting antenna gain calculations are presented herein for thick and thin plasma sheath conditions. The rectangular aperture is assumed to be terminated in an infinite ground plane and dielectrically filled as shown in Fig. 1. The inhomogeneous plasma covering the ground plane is approximated by a number of equivalent slabs.

The equivalent circuit representing the antenna matching network is shown in Fig. 2. The lossy waveguide section approximates the antenna window; the ideal transformer and tuning reactance represents a coax-to-waveguide transition. The probe antenna is assumed to be thin and loosely coupled to the waveguide cavity. A similar problem was considered by Adams (Ref. 1) for free-space conditions only. The actual circuit parameters required for various tuning conditions may not be realizable from a practical standpoint; however, the results illustrate the magnitude of the feeding network effects.



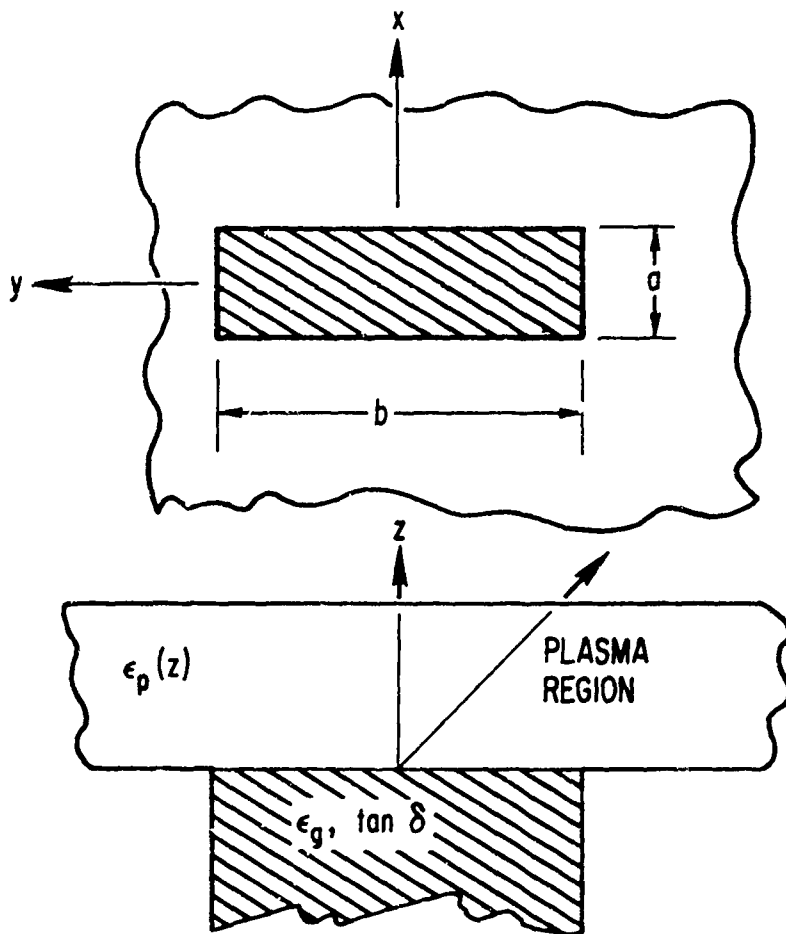
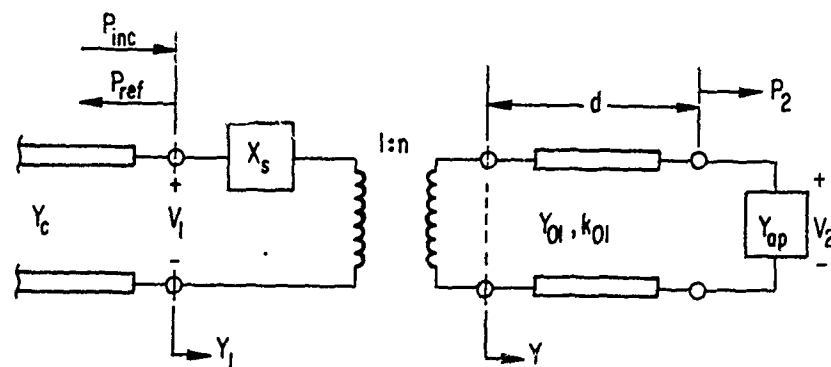
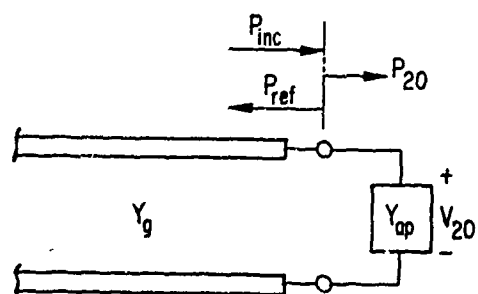


Figure 1. Slot Geometry



(a) FEED NETWORK



(b) FREE EXCITATION

Figure 2. Feed Network

## II. APERTURE ADMITTANCE

The aperture admittance was calculated for various plasma conditions for the aperture configuration shown in Fig. 1. If the reaction concept (Ref. 2) and the dominant mode approximation are used, the aperture admittance can be written as

$$\frac{Y_{ap}}{Y_0} = \frac{\iint [\bar{E}_T(z=0) \times \bar{H}_T(z=0)] \cdot d\bar{S}}{Y_0 V_0^2} \quad (1)$$

where  $\bar{E}_T(z=0)$  is the tangential aperture electric field,  $\bar{H}_T(z=0)$  is the tangential aperture magnetic field,  $Y_0$  is the characteristic admittance of free space, and  $V_0$  is the dominant mode voltage. For the aperture orientation shown in Fig. 1, the dominant mode aperture electric field is

$$\bar{E}_T(z=0) = V_0 (2/ab)^{1/2} \cos(\pi y/b) \bar{a}_x \quad (2)$$

where  $a$  is the height of the aperture,  $b$  is the aperture width, and  $\bar{a}_x$  is the unit vector in the  $x$  direction. The above integral can be transformed by Parseval's theorem to a two-dimensional integral in Fourier transform space. If the transform fields are separated into  $TE_z$  and  $TM_z$  components, the resulting aperture-admittance expression is

$$\frac{Y_{ap}}{Y_0} = \frac{\iint_{-\infty}^{+\infty} |\xi_T^S(k_x, k_y)|^2 Y_{yx} dk_x dk_y}{V_0^2 Y_0} \quad (3)$$

$$Y_{yx} = \frac{Y_{TE}^N k_y^2 + Y_{TM}^N k_x^2}{k_y^2 + k_x^2}$$

where  $\xi_T^S(k_x, k_y)$  is the dominant mode aperture electric field Fourier transform,  $Y_{TE}^N$  is the input  $TE_z$  admittance function, and  $Y_{TM}^N$  is the input  $TM_z$  admittance function. The aperture Fourier transform for a rectangular aperture is

$$\xi_T^S = \frac{V_0}{\pi} \left(\frac{ab}{8}\right)^{1/2} \frac{\sin u_1}{u_1} \left( \frac{\sin u_2}{u_2} + \frac{\sin u_3}{u_3} \right) \quad (4)$$

where

$$u_1 = 0.5 (k_x a) \quad (5a)$$

$$u_2 = 0.5 (k_y b + \pi) \quad (5b)$$

$$u_3 = 0.5 (k_y b - \pi) \quad (5c)$$

The TE and TM admittance functions for collisional plasma sheaths were evaluated using a multislabs approximation and standard transmission line theory (Ref. 3).

The resulting input admittances to the  $n^{\text{th}}$  slab are given by

$$\frac{Y_{TE}^n}{Y_0} = \frac{(Y_{TE}^{n-1}/Y_0) \cos(k_z^n \ell_n) + j(k_z^n/k_0) \sin(k_z^n \ell_n)}{\cos(k_z^n \ell_n) + j(Y_{TM}^{n-1} k_0/Y_0 k_z^n) \sin(k_z^n \ell_n)} \quad (6a)$$

$$\frac{Y_{TM}^n}{Y_0} = \frac{(Y_{TM}^{n-1}/Y_0) \cos(k_z^n \ell_n) + j(k_0 \epsilon_n/k_z^n) \sin(k_z^n \ell_n)}{\cos(k_z^n \ell_n) + j(Y_{TE}^{n-1} k_z^n/Y_0 k_0 \epsilon_n) \sin(k_z^n \ell_n)} \quad (6b)$$

where  $k_z^n$  is defined as

$$k_z^n = k_0 (\epsilon_n - k_x^2/k_0^2 - k_y^2/k_0^2)^{1/2} \quad (7)$$

and  $\epsilon_n$  is the complex relative dielectric constant of the  $n^{\text{th}}$  slab,  $l_n$  is the thickness of the  $n^{\text{th}}$  slab, and  $k_0$  is the free space wavenumber. If the radiation condition is imposed, the admittances at the outer plasma surface are

$$Y_{\text{TE}}^0/Y_0 = k_z^0/k_0 \quad (8a)$$

$$Y_{\text{TM}}^0/Y_0 = k_0/k_z^0 \quad (8b)$$

where  $k_z^0$  is

$$k_z^0 = \beta_z^0 - j\alpha_z^0 = k_0 (1 - k_x^2/k_0^2 - k_y^2/k_0^2)^{1/2} \quad (9)$$

The TE and TM admittances of the aperture surface were evaluated by starting at the outer plasma boundary and transforming the load admittances given in Eqs. (8) through the N-plasma slabs using Eqs. (6). A more detailed description of the analysis and the numerical integration of Eq. (3) is given in Ref. 3. A summary of self- and mutual-admittance calculations compared with plasma simulation measurements is given in Ref. 4. The actual numerical results are presented in Section V.

When the thin sheath approximation is valid, the aperture admittance can be approximated by (Refs. 3 and 5)

$$Y_{\text{ap}} = Y_{\text{ap}}^0 + Y_s \quad (10)$$

where  $Y_{\text{ap}}^0$  is the aperture admittance in free space, and  $Y_s$  is the equivalent plasma surface admittance

$$Y_s = jY_0 k_0 \epsilon_p(\text{peak}) \int \frac{N_e(z) dz}{N_e(\text{peak})} \quad (11)$$

The electron density is  $N_e(z)$ , and the relative dielectric constant at the peak electron density conditions in the sheath is  $\epsilon_p(\text{peak})$ .

### III. ANTENNA GAIN

For purposes of this discussion the antenna gain of a slot antenna radiating through a plasma sheath is defined as

$$g(\theta, \phi) = \frac{2\pi r^2 Y_0}{P_{inc}} \left\{ |E_\theta(r, \theta, \phi)|^2 + |E_\phi(r, \theta, \phi)|^2 \right\} \quad (12)$$

where  $P_{inc}$  is the forward or incident power to the antenna-feed system,  $E_\theta$  is the far field theta component of the electric field, and  $E_\phi$  is the far field phi component of the electric field. The spherical coordinates are denoted by  $r, \theta$ , and  $\phi$ . It is well known that the far field radiation from a slot antenna can be related to the Fourier transform of the aperture field. In the case of a plasma or dielectric covered antenna, the far field is related to the Fourier transform of the electric field at the outer plasma surface. The far field components are obtained using saddle-point integration techniques, resulting in

$$E_\theta(r, \theta, \phi) = j \frac{2\pi}{r\lambda_0} \cos\phi \frac{\xi_T^S(k_{xs}, k_{ys})}{G_{TM}(k_{xs}, k_{ys})} \exp(-jk_0 r) \exp(+jk_0 \cos\theta \sum_{n=1}^N l_n) \quad (13a)$$

$$E_\phi(r, \theta, \phi) = -j \frac{2\pi}{r\lambda_0} \sin\phi \cos\theta \frac{\xi_T^S(k_{xs}, k_{ys})}{G_{TE}(k_{xs}, k_{ys})} \exp(-jk_0 r) \exp(+jk_0 \cos\theta \sum_{n=1}^N l_n) \quad (13b)$$

where Fourier transform functions are evaluated at

$$k_{xs} = k_0 \sin\theta \cos\phi \quad (14a)$$

$$k_{ys} = k_0 \sin\theta \sin\phi \quad (14b)$$

$$k_{zs}^n = k_0 (\epsilon_n - \sin^2\theta)^{1/2} \quad (14c)$$

The resulting gain expression is

$$g(\theta, \phi) = \frac{8k_0^2 ab Y_0}{\pi^3 Y_c} |V_{ap}/V_{inc}|^2 P_e(\theta, \phi) \quad (15)$$

where the radiation pattern  $P_e(\theta, \phi)$  is given by

$$P_e(\theta, \phi) = \frac{\pi^2}{16} \left[ \frac{\sin u_{1s}}{u_{1s}} \left( \frac{\sin u_{2s}}{u_{2s}} + \frac{\sin u_{3s}}{u_{3s}} \right) \right]^2 \left[ \frac{\cos^2 \phi}{|G_{TM}(\theta)|^2} + \frac{\sin^2 \phi \cos^2 \theta}{|G_{TE}(\theta)|^2} \right] \quad (16)$$

and the aperture voltage, incident voltage, and characteristic admittance of the feed transmission line are denoted by  $V_{ap}$ ,  $V_{inc}$ , and  $Y_c$ , respectively.

The functions  $u_{1s}$ ,  $u_{2s}$ , and  $u_{3s}$  are defined in Eqs. (5) with

$$k_x = k_{xs} \text{ and } k_y = k_{ys}$$

$$u_{1s} = 0.5 (k_0 a \sin \theta \cos \phi) \quad (17a)$$

$$u_{2s} = 0.5 (k_0 b \sin \theta \sin \phi + \pi) \quad (17b)$$

$$u_{3s} = 0.5 (k_0 b \sin \theta \sin \phi - \pi) \quad (17c)$$

The radiation pattern is normalized to unity at broadside ( $\theta = 0$ ) when the slot is radiating into free space.

The TE and TM components of the aperture electric field Fourier transform  $\xi_T^S(k_x, k_y, z=0)$  were transformed to the outer plasma surface by the plasma distortion functions  $G_{TE}$  and  $G_{TM}$ , respectively.

The distortion functions are defined as

$$G_{TE} = \left[ \bar{a}_{TE} \cdot \bar{a}_x \xi_T^S(z=0) \right] / \left[ \bar{a}_{TE} \cdot \bar{\xi}_T \left( z = \sum_1^N \ell_n \right) \right] \quad (18a)$$

$$G_{TM} = \left[ \bar{a}_{TM} \cdot \bar{a}_x \xi_T^S(z=0) \right] / \left[ \bar{a}_{TM} \cdot \bar{\xi}_T \left( z = \sum_1^N \ell_n \right) \right] \quad (18b)$$

where  $\bar{a}_{TE}$  and  $\bar{a}_{TM}$  are the  $TE_z$  and  $TM_z$  mode unit vectors

$$\bar{a}_{TE} = (\bar{a}_x k_y - \bar{a}_y k_x) / (k_x^2 + k_y^2)^{1/2} \quad (19a)$$

$$\bar{a}_{TM} = (\bar{a}_x k_x + \bar{a}_y k_y) / (k_x^2 + k_y^2)^{1/2} \quad (19b)$$

The transverse electric field Fourier transform at the outer plasma surface is denoted by  $\bar{\xi}_T(z = \sum_1^N \ell_n)$ . For the multislabs approximation the distortion functions are

$$G_{TE}(\theta) = \prod_{n=1}^N \left[ \cos(k_{zs}^n \ell_n) + j(Y_{TE}^{n-1} k_0 / Y_0 k_{zs}^n) \sin(k_{zs}^n \ell_n) \right] \quad (20a)$$

$$G_{TM}(\theta) = \prod_{n=1}^N \left[ \cos(k_{zs}^n \ell_n) + j(Y_{TM}^{n-1} k_{zs}^n / Y_0 k_0 \epsilon_n) \sin(k_{zs}^n \ell_n) \right] \quad (20b)$$

The admittance functions are defined in Eqs. (6).

For a freely excited slot antenna (Fig. 2b), the aperture voltage can be expressed in terms of the aperture admittance. The resulting aperture gain is given by

$$g_{ap}(\theta, \phi) = \frac{8k_0^2 a b}{\pi^3} \frac{Y_0}{Y_g} |1 + \rho_{ap}|^2 P_e(\theta, \phi) \quad (21)$$



where the aperture reflection coefficient is

$$\rho_{ap} = \frac{Y_g - Y_{ap}}{Y_g + Y_{ap}} \quad (22)$$

and the waveguide characteristic admittance is

$$Y_g = Y_0 \left[ \epsilon_g - (\pi/k_0 b)^2 \right]^{1/2} \quad (23)$$

When the aperture is excited by a feed network (Fig. 2a) the net antenna gain, including feed absorption and input reflections, can be expressed as

$$g_F(\theta, \phi) = \frac{8k_0^2 a b Y_0}{\pi^3 Y_c} \left| \frac{V_2}{V_1} \right|^2 |1 + \rho_F|^2 P_e(\theta, \phi) \quad (24)$$

where the reflection coefficient at the input terminals of the feed is

$$\rho_F = \frac{Y_c - Y_1}{Y_c + Y_1} \quad (25)$$

In Eq. (25),  $Y_c$  is the characteristic admittance of the input transmission line;  $Y_1$  is the input admittance to the feed, and is determined from a circuit analysis of the feed. In Eq. (24)  $V_2/V_1$  is the voltage transfer function of the feed. Subscripts F and ap [Eqs. (21), (22), and (24)] designate the feed and aperture, respectively.

When the plasma is in contact with the ground plane and the thin sheath limit is valid, the distortion functions are equal to unity. The resulting radiation patterns are equal to the free space patterns, and the antenna gain is reduced by the reflection loss only.

#### IV. FEED NETWORK

The hypothetical feed equivalent circuit is shown in Fig. 2a. The aperture admittance is transformed through the heat shield to the output terminals of an ideal transformer representing a coax-to-waveguide transition by a length of lossy waveguide having the same cross-sectional dimensions of the aperture. The dielectric constant and cross-sectional dimensions of the dielectrically loaded waveguide are selected in such a way that only the  $TE_{01}$  mode propagates. The transformer turn ratio  $n$  and series reactance  $X_s$  are adjusted to obtain the desired antenna matching.

The admittance at the terminal plane of the transformer looking toward the aperture is given by

$$\frac{Y}{Y_{01}} = \frac{(Y_{ap}/Y_{01}) \cos(k_{01}d) + j \sin(k_{01}d)}{\cos(k_{01}d) + j(Y_{ap}/Y_{01}) \sin(k_{01}d)} \quad (25)$$

where the complex propagation constant and characteristic admittance of the  $TE_{01}$  waveguide mode are equal to

$$Y_{01} = Y_0 \left[ \epsilon_g (1 - j \tan \delta) - (\pi/k_0 b)^2 \right]^{1/2} \quad (26a)$$

$$k_{01} = k_0 \left[ \epsilon_g (1 - j \tan \delta) - (\pi/k_0 b)^2 \right]^{1/2} \quad (26b)$$

The input admittance and aperture voltage were obtained from a simple network. The results are given by

$$Y_1 = \frac{Y_n^2}{1 + j Y_n^2 X_s} \quad (27a)$$

$$\frac{V_2}{V_1} = \frac{n}{(1 + j Y_n^2 X_s) G_{01}(k_{01}d)} \quad (27b)$$

$$G_{01}(k_{01}d) = \cos(k_{01}d) + j(Y_{ap}/Y_{01})\sin(k_{01}d) \quad (27c)$$

where  $G_{01}(k_{01}d)$  is the voltage transfer function that relates the aperture to the voltage at the transformer end of the waveguide.

The aperture-feed combination was matched by adjusting the turn ratio and series reactance until the reflections at the input terminals were reduced to zero. For a specified aperture admittance, the matched conditions were obtained by setting

$$n^2 = \text{Real}(Y_c/Y) \quad (28a)$$

$$\frac{X_s}{Z_c} = + \frac{\text{imag}(Y)}{\text{Real}(Y)} \quad (28b)$$

where the characteristic impedance of the input transmission line is  $Z_c = Y_c^{-1}$ . The matching equations were obtained by setting  $Y_1 = Y_c$  in Eq. (27a).

## V. NUMERICAL RESULTS

The antenna admittance, antenna gain, input voltage standing wave ratio (VSWR), and plane wave attenuation computations are presented for various plasma conditions at S-band frequencies.

The dimensions of the aperture, dielectric properties of the window, and length of the waveguide window are given in Table 1.

Table 1. Physical Dimensions of Waveguide Window

Case	$k_0 a$	$k_0 b$	$\epsilon_g$	$\tan \delta$	$d/\lambda_g$	$Z_c$ , ohm
1	0.45	2.10	4.0	0.01	0.5	50
2	0.45	2.10	4.0	0.04	0.5	50

The physical dimensions are typical of proposed S-band telemetry antenna systems.

The normalized electron density profile used in the calculations is shown in Fig. 3. The peak electron density was varied from  $2.5 \times 10^{11}$  to  $7.2 \times 10^{12} \text{ cm}^{-3}$ . The plasma was approximated by eight equivalent slabs that provided adequate numerical accuracy at S-band frequencies. The collision frequency was assumed to be constant and equal to  $6 \times 10^9$  collisions per second.

### A. APERTURE ADMITTANCE

The aperture admittance calculations were obtained by numerically integrating Eq. (3). The results are normalized to the free admittance  $Y_0$  and are plotted on the Smith chart shown in Fig. 4. Thin sheath results using Eq. (10) are also plotted in Fig. 4 for various equivalent surface resistances. The thin sheath results approximate thin, highly overdense, collision-dominated plasma sheaths typically encountered at low altitudes on slender conical

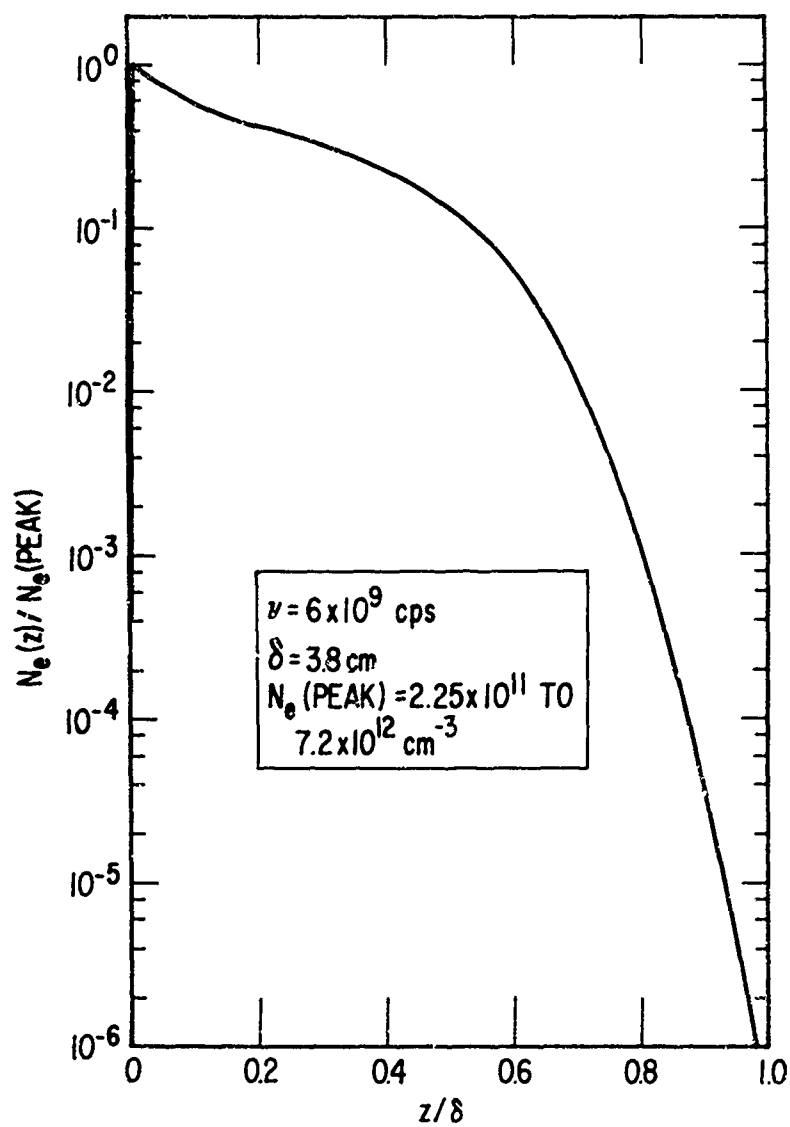


Figure 3. Reentry Plasma Sheath



vehicles. The thin sheath results also approximate the results obtained if the antenna aperture is covered with a resistive cloth, commonly called space cloth. The numbers adjacent to the thick slab calculations (Fig. 4) denote peak electron density; the numbers adjacent to the thin sheath results denote the additive surface resistance. Because of the small size of the aperture, the open-ended waveguide aperture behaves as an open circuit in free space and as a short circuit in the plasma.

#### B. FREE EXCITATION ANTENNA GAIN

The antenna gain can be calculated using Eqs. (21) through (23) when the aperture is waveguide-fed with an isolator absorbing the aperture reflections. The E-plane ( $\theta = 0^\circ$ ) results are plotted in Fig. 5. The aperture is loaded with a dielectric having a dielectric constant equal to 4.0 and  $\tan\delta = 0$ . The H-plane calculations are shown in Fig. 6. The angle theta is measured from the aperture normal or z-axis (Fig. 1). The numbers adjacent to the curves (Figs. 5 and 6) denote the peak electron density conditions in units of  $\text{cm}^{-3}$ . The radiation pattern distortions induced by the plasma are evident by comparing the free space gain with the corresponding antenna gain calculations in the presence of the plasma. However, the most predominant plasma-antenna effect shown in Figs. 5 and 6 is signal attenuation.

#### C. FEED CALCULATIONS

The insertion loss ratio of the feed network is defined as

$$\text{Insertion loss} = P_2/P_{20} \quad (29a)$$

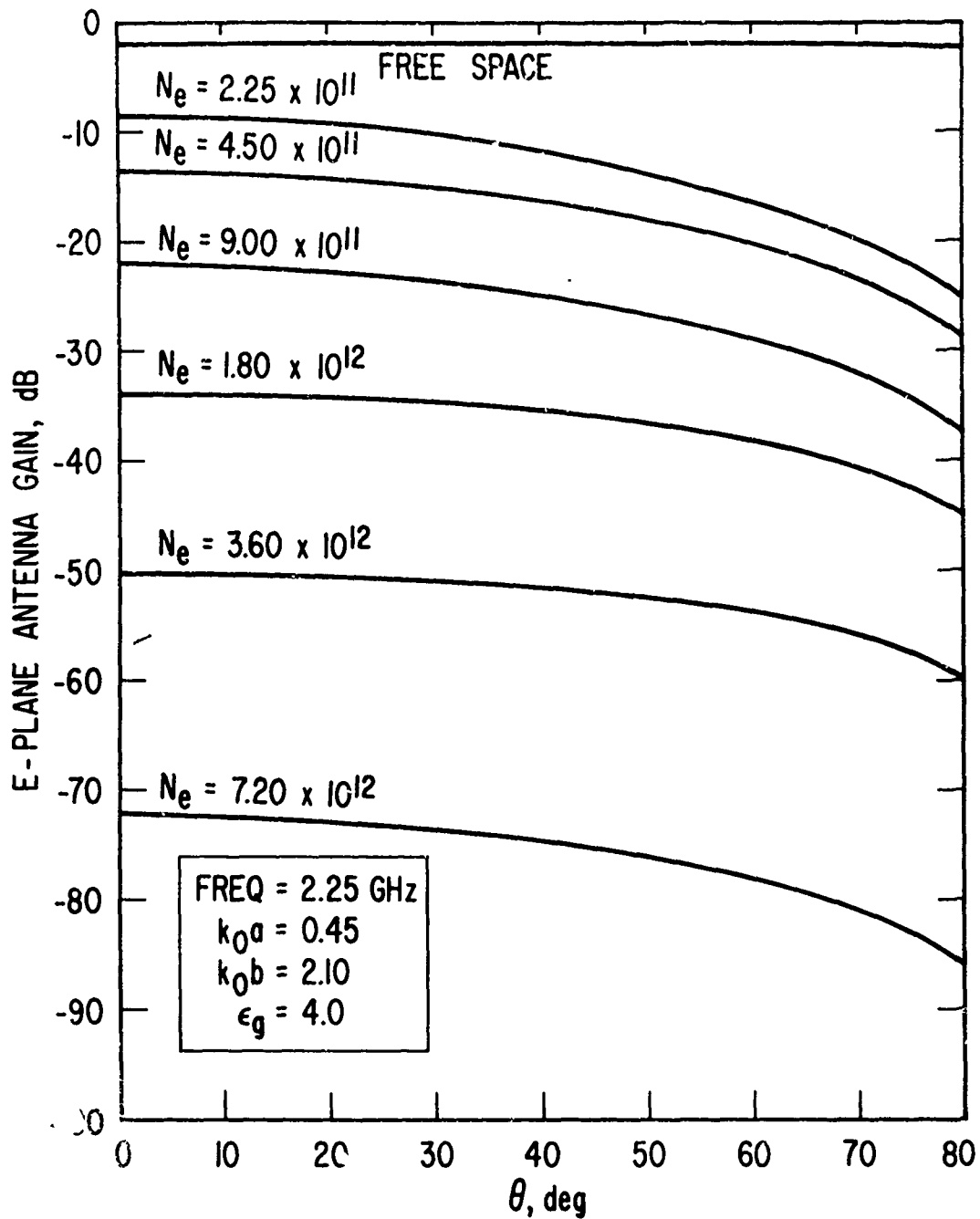


Figure 5. E-Plane Antenna Gain



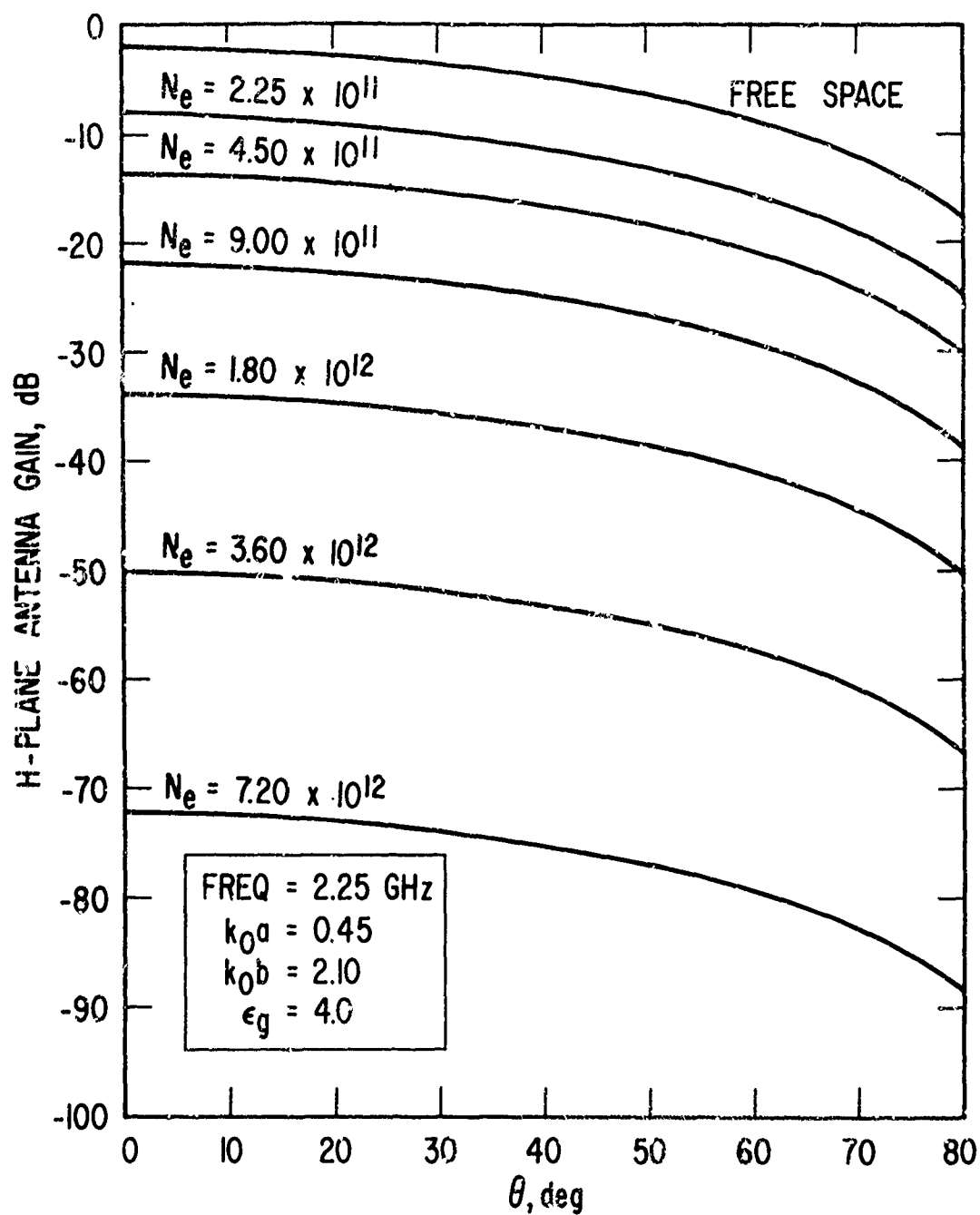


Figure 6. H-Plane Antenna Gain

where

$$\frac{P_2}{P_{inc}} = \frac{\text{Real}(Y_{ap})}{Y_c} \left| \frac{V_2}{V_1} \right|^2 |1 + \rho_F|^2 \quad (29b)$$

$$\frac{P_{20}}{P_{inc}} = \frac{\text{Real}(Y_{ap})}{Y_g} |1 + \rho_{ap}|^2 \quad (29c)$$

The insertion loss can be reduced to

$$\frac{P_2}{P_{20}} = \frac{Y_g}{Y_c} \left| \frac{V_2}{V_1} \right|^2 \frac{|1 + \rho_F|^2}{|1 + \rho_{ap}|^2} \quad (30)$$

The above nomenclature is defined in Fig. 2. This particular definition of insertion loss is useful since the net antenna, including the feed, is expressed as

$$g_F(\theta, \phi) = (P_2/P_{20}) g_{ap}(\theta, \phi) \quad (31)$$

The results of the insertion loss calculations are shown in Fig. 7. The antenna-feed system was matched to free space conditions. The results for two loss tangent values are presented. The reflection loss for the same matching conditions are plotted in Fig. 8. The reflection loss shown in Fig. 8 is defined as

$$\text{Reflection loss} = 1 - |\rho_F|^2 \quad (32)$$

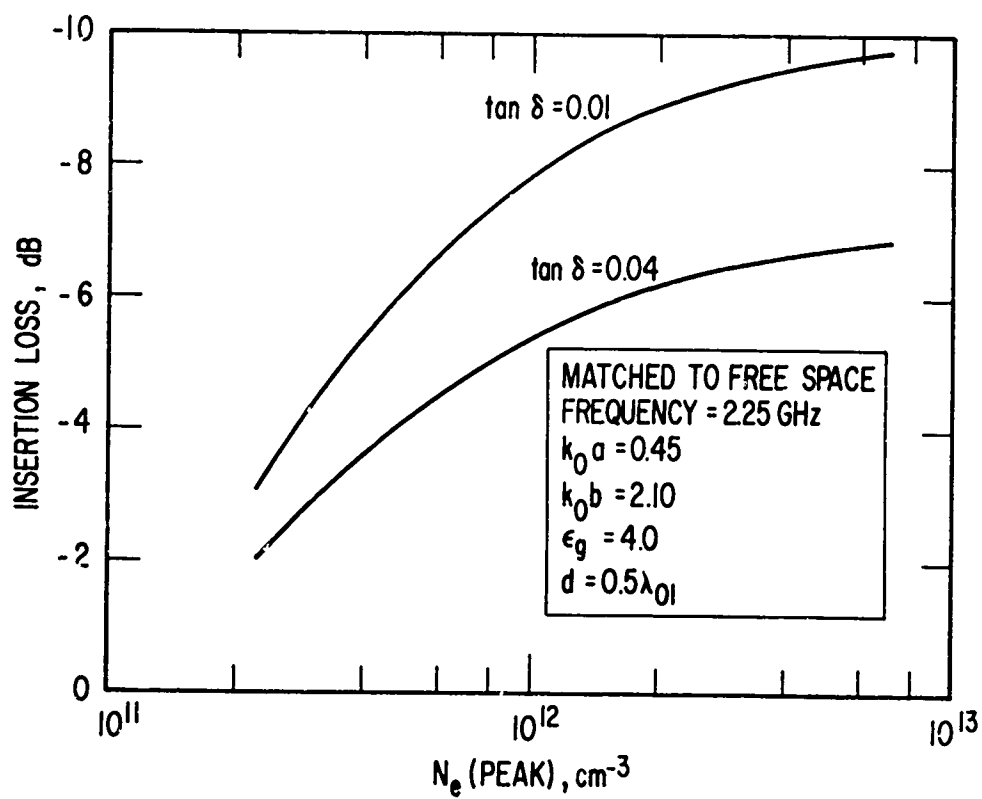


Figure 7. Feed Network Insertion Loss

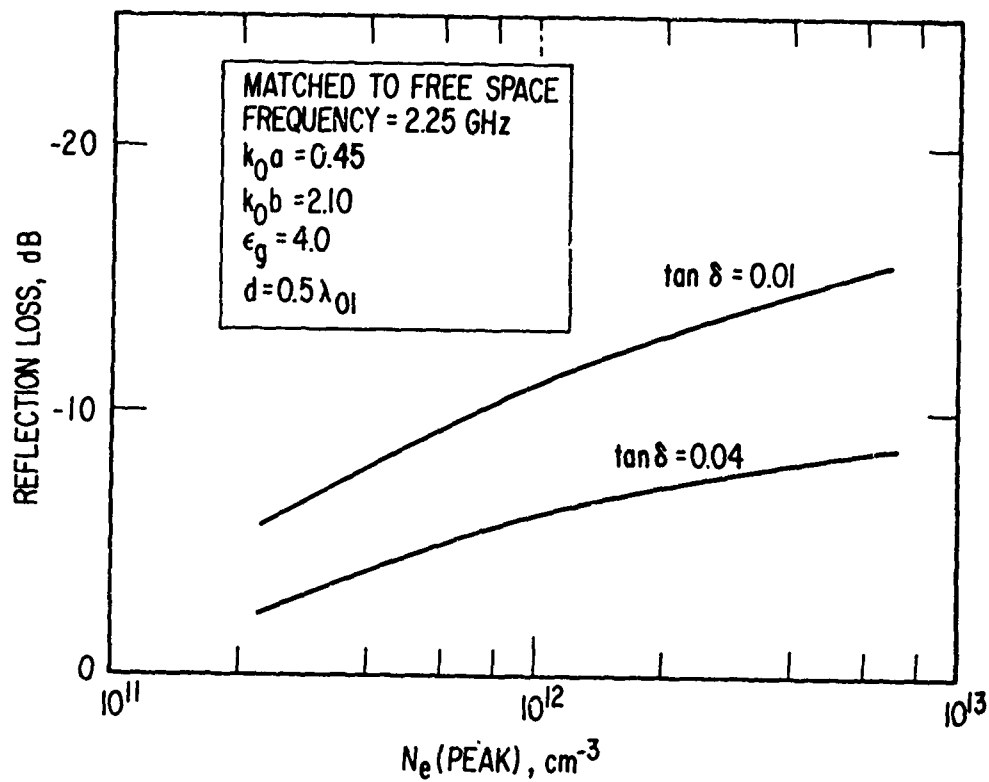


Figure 8. Reflection Loss vs Electron Density

The total antenna-feed system degradation caused by the reentry plasma is best illustrated by comparing inhomogeneous plane wave attenuation predictions with the change in broadside antenna gain induced by the plasma. The change in antenna gain is defined as

$$\Delta\text{Gain} = g_F^P(\theta = 0)/g_F^0(\theta = 0) \quad (33)$$

where  $g_F^P(\theta = 0)$  is the total antenna gain in the plasma environment and  $g_F^0(\theta = 0)$  is the free space antenna gain. The turn ratio and series reactance were selected to match the system to a free space environment. The relative gain expression given in Eq. (33) was therefore a measure of the telemetry link degradation caused by the plasma and/or changing the matching conditions. In Fig. 9 the plane wave attenuation and  $\Delta\text{Gain}$  calculations are shown as a function of peak electron density. The most important effect to note is the large difference between the antenna calculations and the commonly used plane wave calculations. The signal attenuation associated with the reflection and absorption losses in the feed are indicated by the difference between the feed results and the free excitation results.

The VSWR at the input terminals is

$$\text{VSWR} = (1 + |\rho_F|)/(1 - |\rho_F|)$$

where the reflection coefficient is given in Eq. (25). The results of the VSWR calculations are shown in Fig. 10, assuming the antenna is matched to free space conditions. The results indicate the absorption effects in the window as the loss tangent is increased.

Since plane wave analyses are commonly used to predict signal attenuation in telemetry link margin computations, the difference between the plane wave attenuation and relative gain calculations shown in Fig. 9

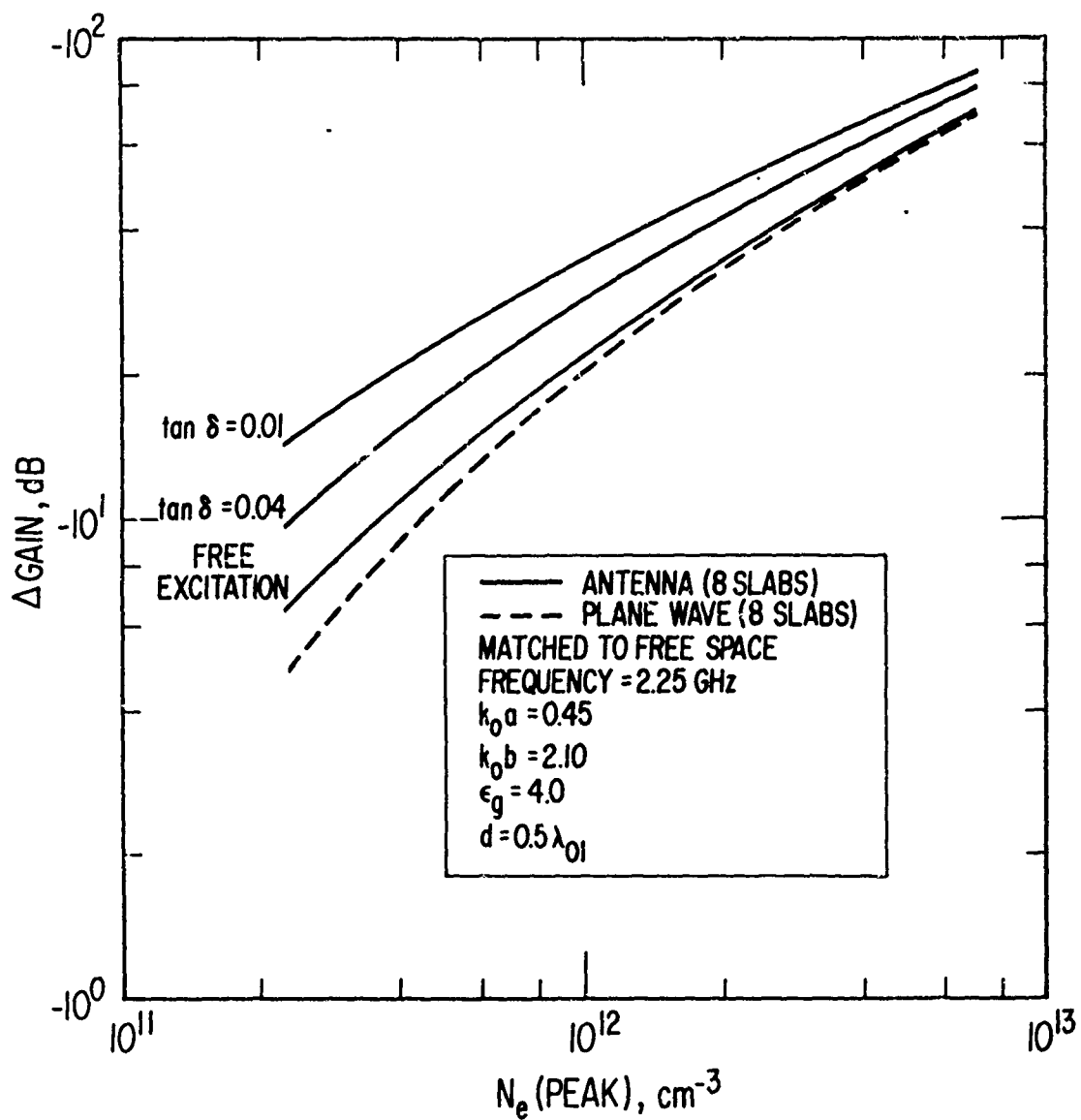


Figure 9. Change in Antenna Gain with Aperture Matched to Free Space

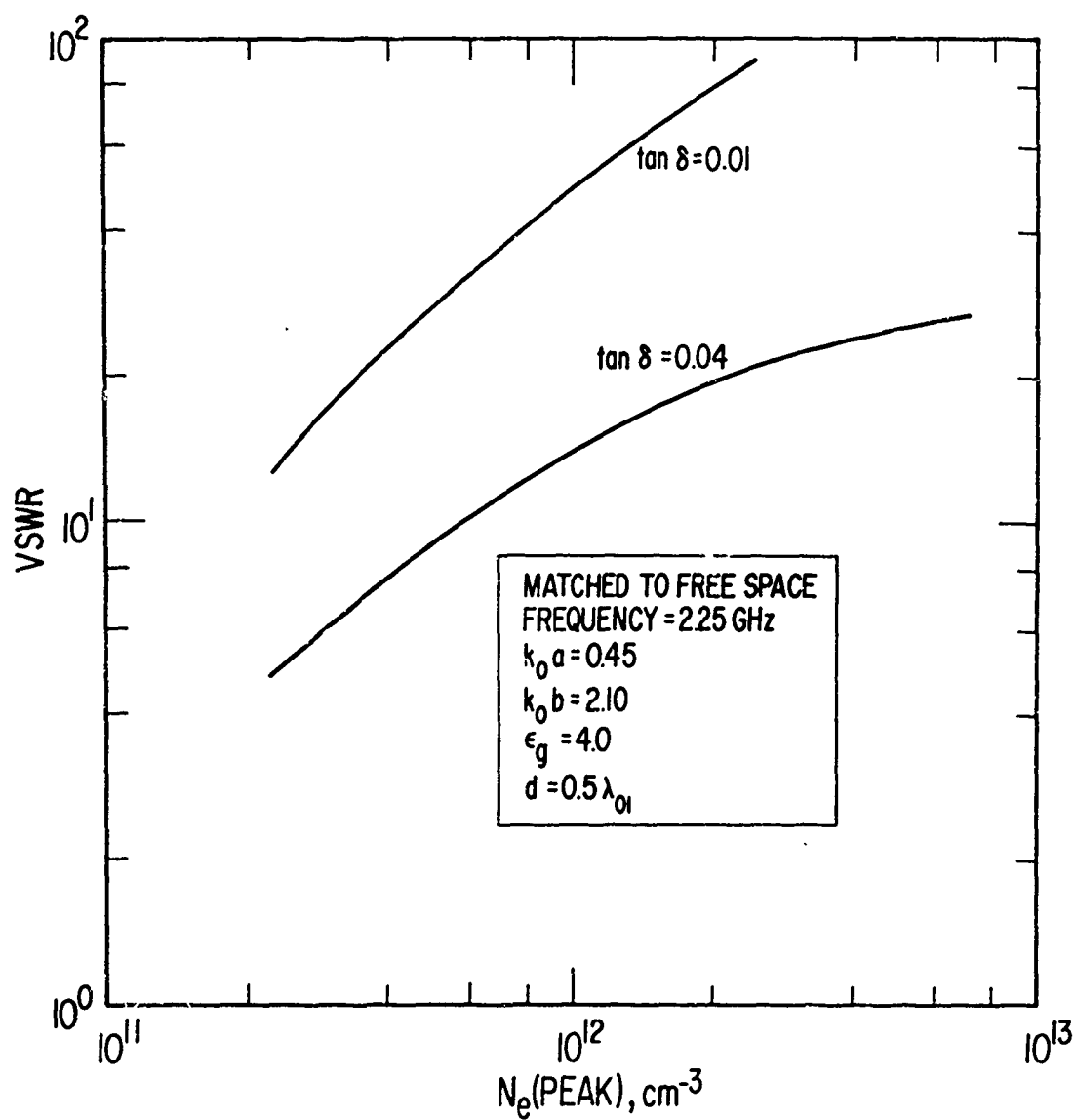


Figure 10. Input VSWR with Aperture Matched to Free Space

is plotted in Fig. 11. The plane wave error is defined as

$$\text{Error} = tt^*/\Delta\text{Gain}$$

where  $tt^*$  is the plane wave transmission coefficient. These results indicate that the plane wave predictions can underestimate signal attenuation by at least 5 to 15 dB. The plane wave analysis does not properly approximate the absorption and reflection losses of the feed and surface wave effects in the plasma.

The thin sheath results are plotted in Figs. 12 and 13. In these cases the aperture admittance was calculated using the asymptotic expression shown in Eqs. (10) and (11). The equivalent surface susceptance was assumed to be zero and the conductance varied from 0.001 mho to 0.1 mho. The results are applicable for low-altitude turbulent plasma sheaths surrounding slender conical vehicles.

#### D. ABSORPTION EFFECTS IN THE WAVEGUIDE ANTENNA WINDOW

The decrease in antenna gain caused by increased window absorption due to temperature effects was obtained by parametrically varying the loss tangent of the waveguide window from 0.01 to 0.16, keeping the turn ratio and series reactance fixed. The feed network was matched to free space conditions with a loss tangent of 0.01. Figure 14 shows the decrease in antenna gain for various plasma conditions. In addition to increased absorption, the reflection loss decreases as the window losses increase (Fig. 15). The decrease in reflection losses from window absorption ultimately limits antenna matching techniques in a reentry environment.



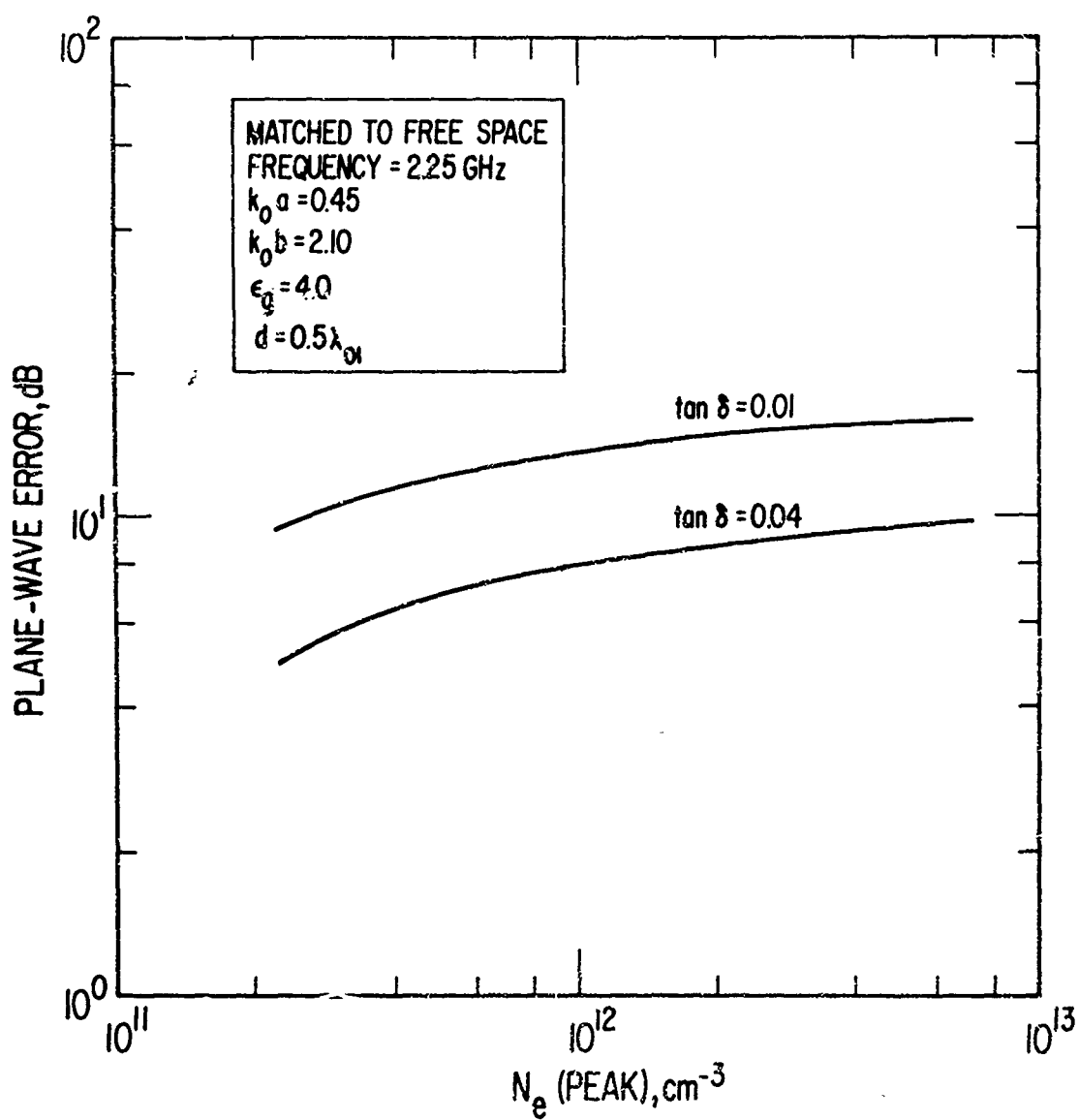


Figure 11. Plane Wave Attenuation Error

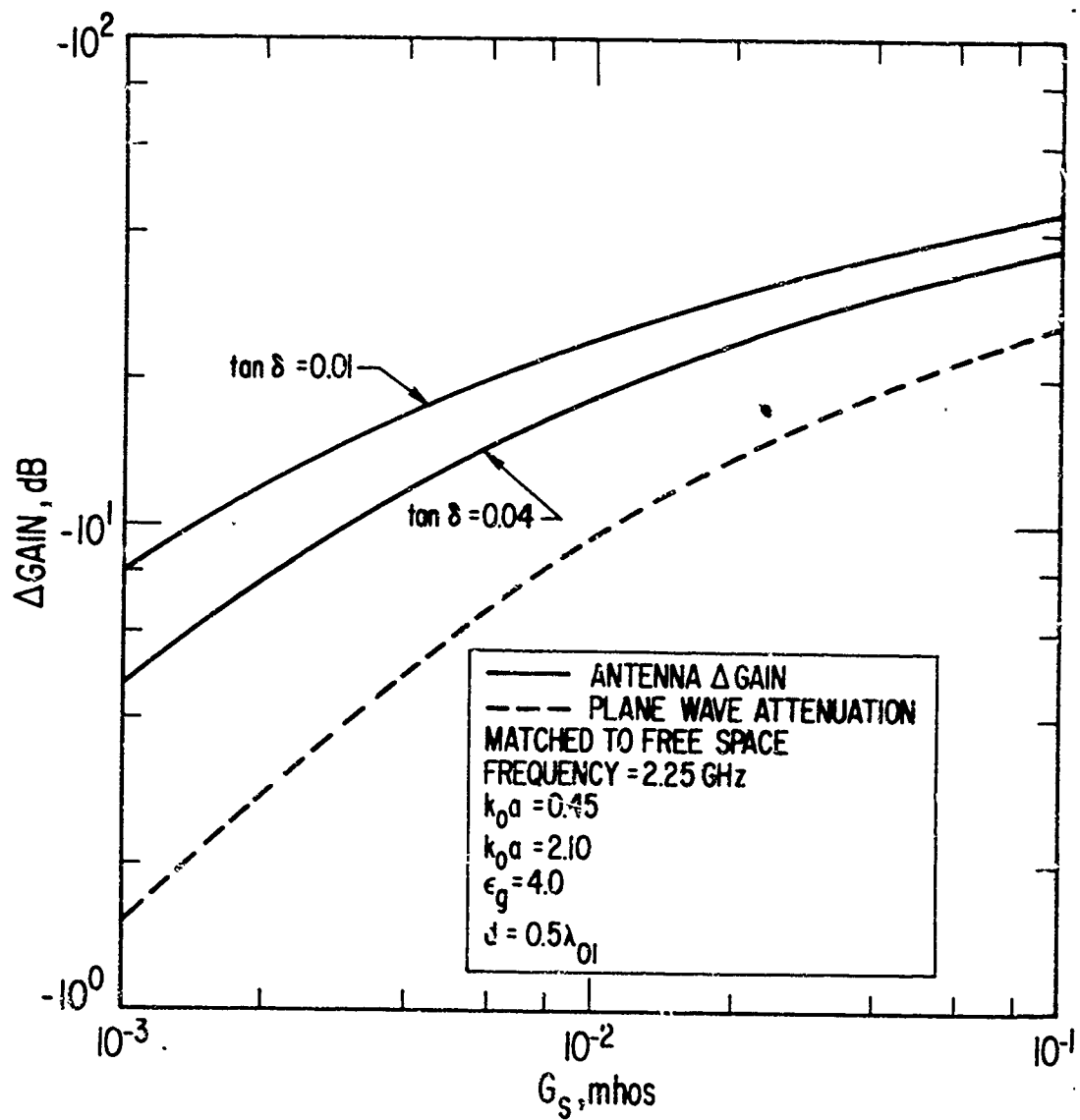


Figure 12. Thin Sheath Limit for Change in Antenna Gain with Aperture Matched to Free Space

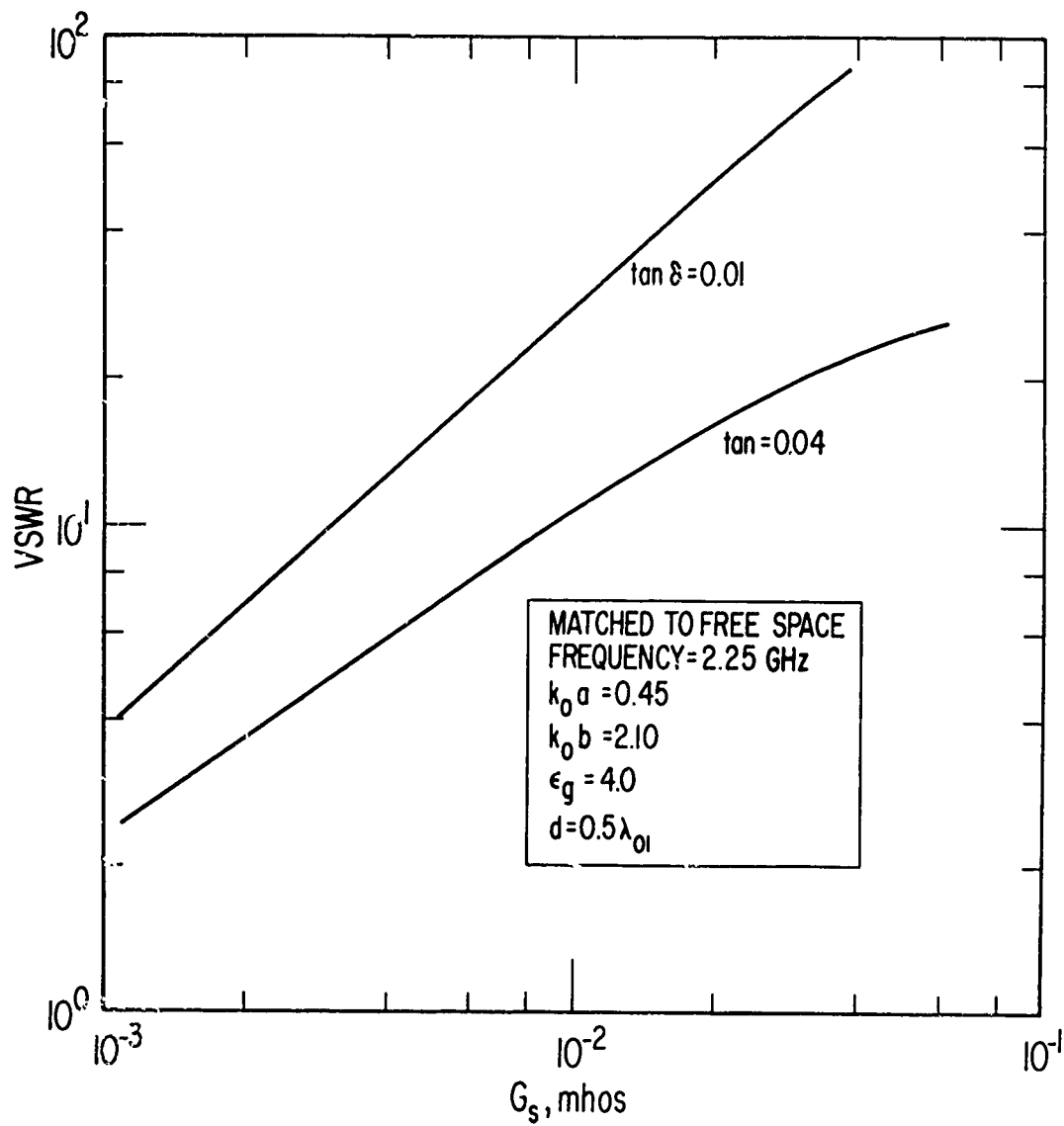


Figure 13. Thin Sheath Limit for Input VSWR with Aperture Matched to Free Space

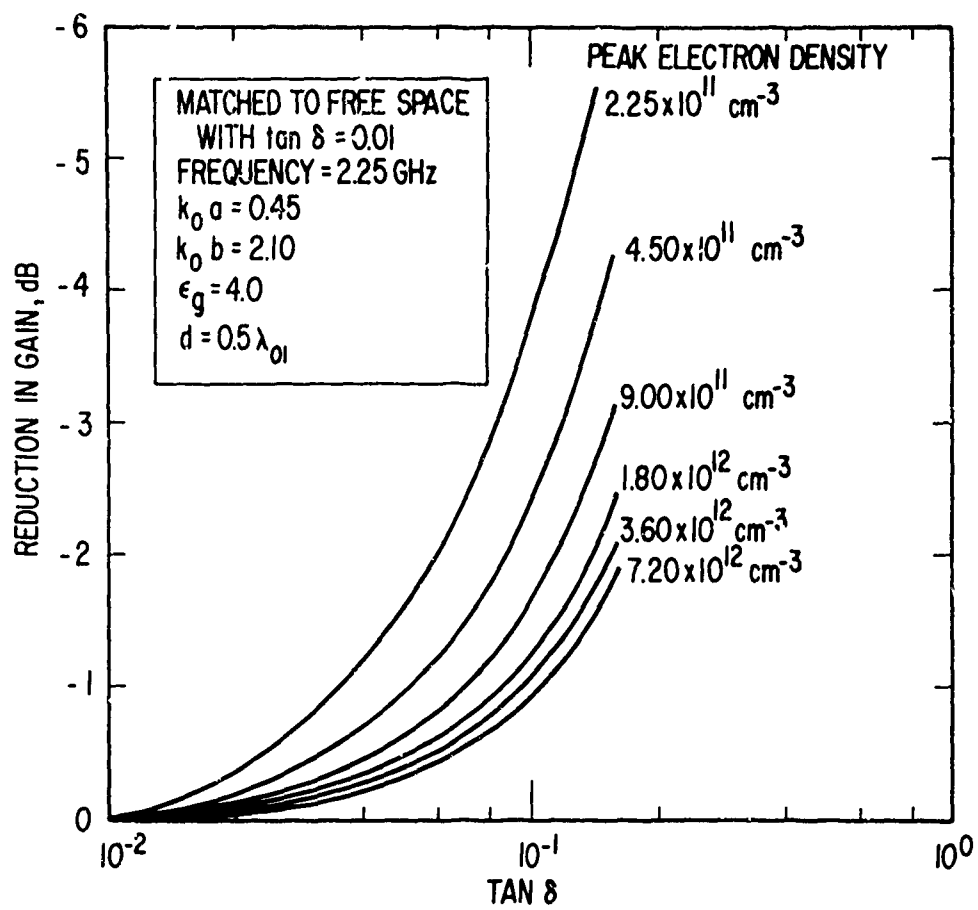


Figure 14. Reduction in Antenna Gain Caused by Window Absorption

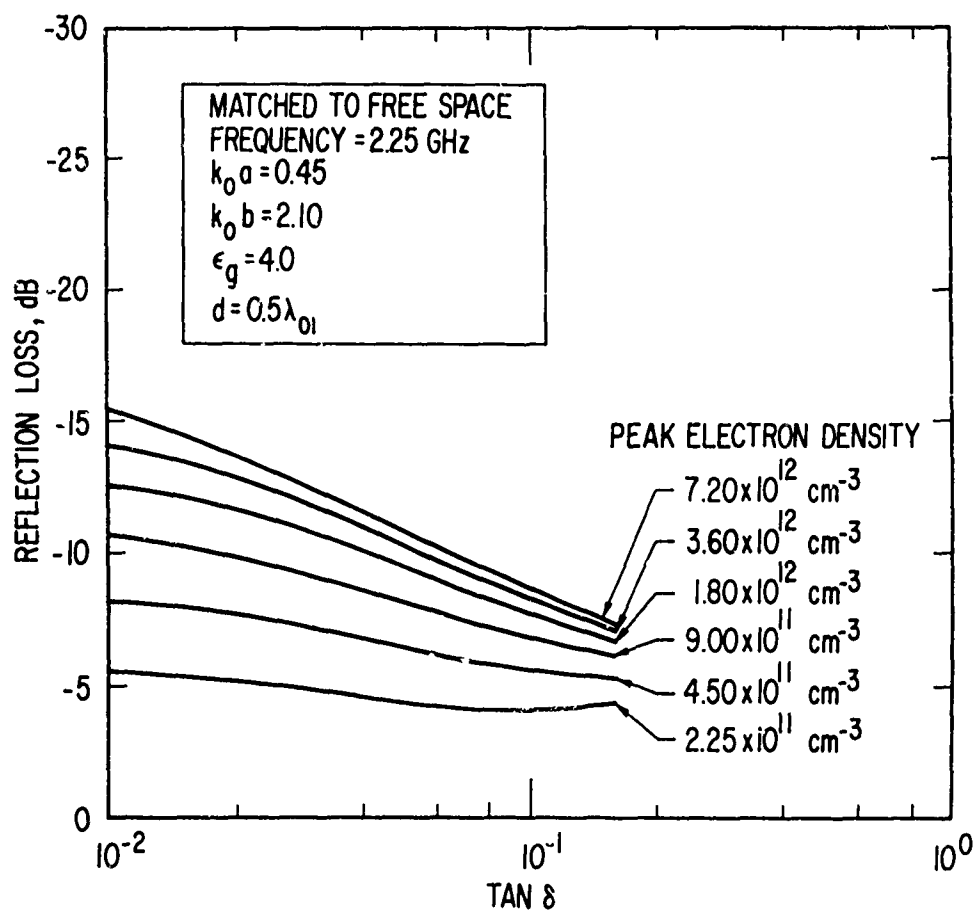


Figure 15. Reflection Loss vs Window Absorption

### E. MATCHING TO A PLASMA ENVIRONMENT

The antenna feed performance under various matching conditions is shown in Figs. 16 through 17, assuming a loss tangent of 0.004. The calculations were performed with the antenna matched to free space conditions, a waveguide load, and  $N_e(\text{peak}) = 5 \times 10^{11} \text{ cm}^{-3}$ . The turn ratio and series reactance were determined, in matching the coax-to-waveguide transition to a nonreflecting waveguide load, by substituting  $Y = Y_{01}$  into Eqs. (28). The turn ratio and series reactance required to match the slot antenna to various conditions are tabulated in Table 2. The input admittance results are plotted in Fig. 16. The resulting  $\Delta\text{Gain}$  calculations are shown in Fig. 17, and the corresponding VSWR results are plotted in Fig. 18. When the antenna was matched to  $N_e(\text{peak}) = 9 \times 10^{11} \text{ cm}^{-3}$ , the antenna gain in free space decreased by 5.8 dB, while the gain at the  $9 \times 10^{11} \text{ cm}^{-3}$  electron density increased by 5.8 dB. As the waveguide window absorption loss increased, the gain improvement decreased. The potential gain improvement resulting from the match at the  $9.0 \times 10^{11} \text{ cm}^{-3}$  electron density was 10.7 dB for a waveguide window loss tangent of 0.01. When the loss tangent was increased to 0.04 the potential gain improvement was decreased to 5.8 dB.

Table 2. Matching Conditions

Antenna Matched to	$\tan\delta$	Turn Ratio	$X_s/Z_c$	$Z_c$ , ohm
Free space	0.01	4.22	-1.54	50
Free space	0.04	4.29	-0.729	50
Waveguide load	0.01	2.38	-0.0113	50
Waveguide load	0.04	2.38	-0.0453	50
$9 \times 10^{11} \text{ cm}^{-3}$	0.01	1.07	-2.72	50
$9 \times 10^{11} \text{ cm}^{-3}$	0.04	1.37	-1.59	50

● MATCHED TO $Y_{01}$	(1) $N_e = 2.25 \times 10^{11} \text{ cm}^{-3}$
△ MATCHED TO FREE SPACE	(2) $N_e = 4.50 \times 10^{11} \text{ cm}^{-3}$
○ MATCHED TO $N_e = 9 \times 10^{11} \text{ cm}^{-3}$	(3) $N_e = 9.00 \times 10^{11} \text{ cm}^{-3}$
FREQUENCY = 2.256 GHz	(4) $N_e = 1.80 \times 10^{12} \text{ cm}^{-3}$
$k_0 a = 0.45$	(5) $N_e = 3.60 \times 10^{12} \text{ cm}^{-3}$
$k_0 b = 2.10$	(6) $N_e = 7.20 \times 10^{12} \text{ cm}^{-3}$
$\epsilon_g = 4.0$	
$\text{TAN } \delta = 0.04$	
$d = 0.5 \lambda_{01}$	

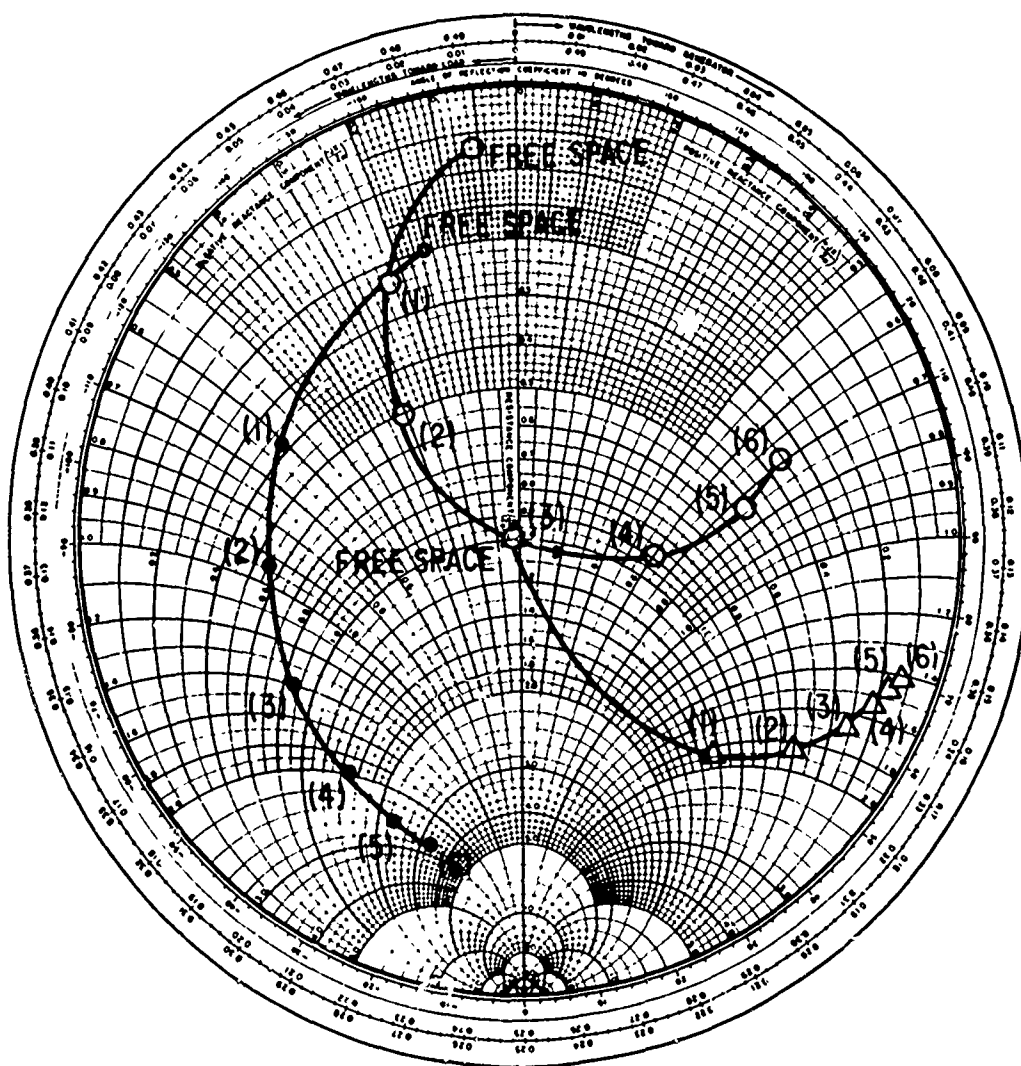


Figure 16. Input Admittance for Various Matching Conditions

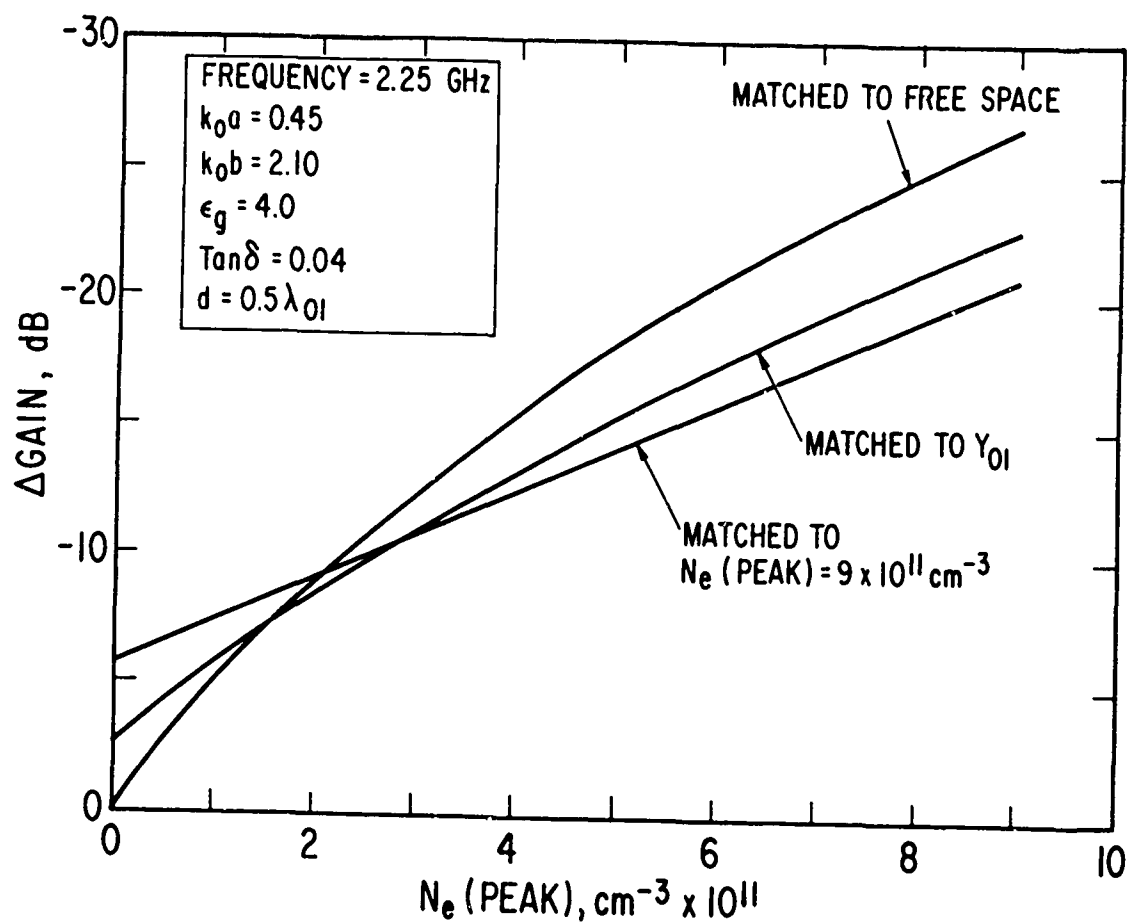


Figure 17. Change in Antenna Gain for Various Matching Conditions



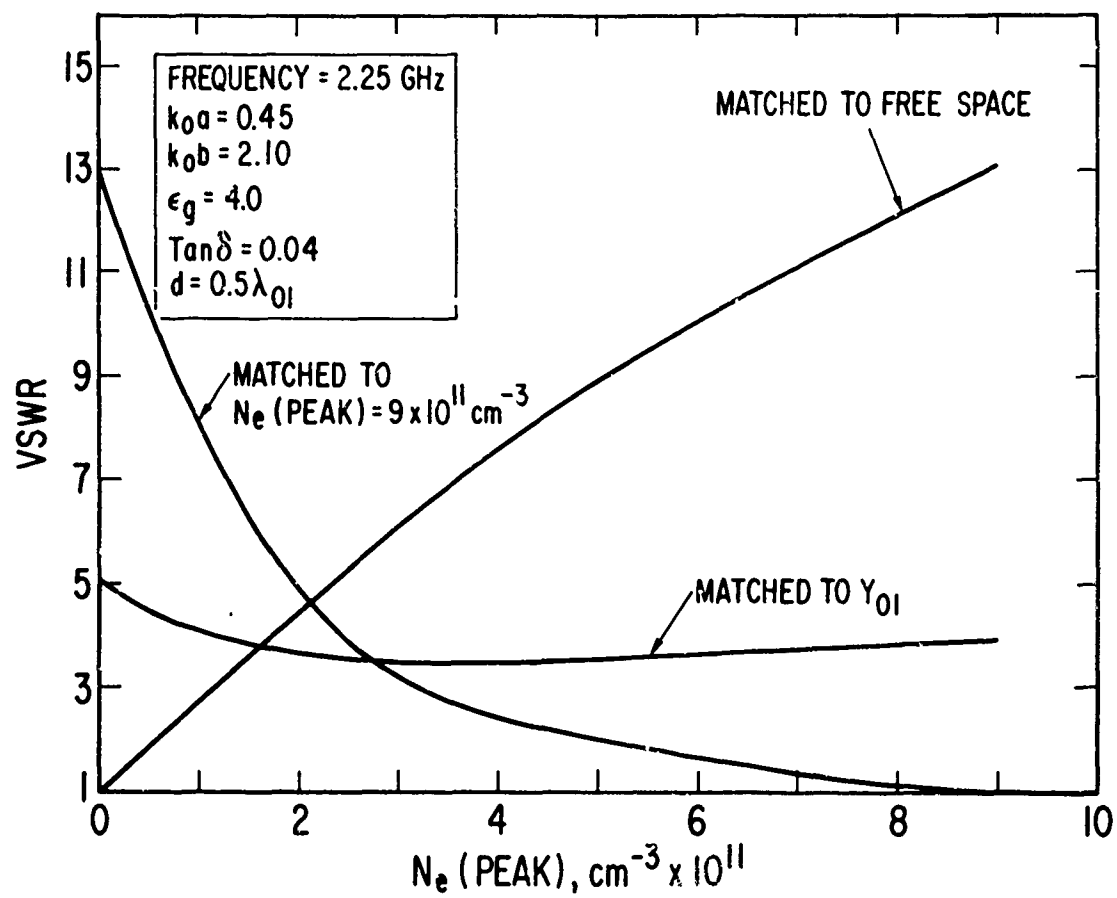


Figure 18. Input VSWR for Various Matching Conditions

## VI. CONCLUSIONS

Antenna gain calculations, including absorption and reflection losses of the feed network are useful in estimating plasma-induced signal attenuation. Plane wave calculations underestimate signal attenuation by 3 to 15 dB at S-band frequencies. As the antenna aperture increases in size, the difference between antenna gain calculations and plane wave predictions decreases. When reflection losses can be neglected in both the plane wave and antenna gain calculations, the attenuation results of both analyses are the same, provided the antenna absorption losses are zero.

The antenna gain in a plasma can be improved by matching the antenna to peak plasma conditions, but at the expense of the free space gain if preset matching is used. As the losses from window absorption losses increase, the amount of gain improvement obtainable by matching decreases. Matching the coax-to-waveguide transition to the characteristic admittance of the waveguide window provides antenna matching midway between the open-circuit conditions of free space and short-circuit conditions of reentry.

## REFERENCES

1. A. T. Adams, "Flush Mounted Rectangular Cavity Slot Antenna - Theory and Design," IEEE Trans. Antennas and Propagation AP-15, 342 (May 1967).
2. R. F. Harrington, Time Harmonic Electromagnetic Fields, McGraw-Hill Book Co., Inc. New York (1969). p. 428.
3. K. E. Golden and G. E. Stewart, Self and Mutual Admittances of Rectangular Slot Antennas in the Presence of an Inhomogeneous Plasma Layer, TR-0200(4220-10)-1, Aerospace Corporation, El Segundo, Calif. (March 1969).
4. K. E. Golden and G. E. Stewart, "Admittance and Isolation of Slot Antennas in the Presence of an Inhomogeneous Plasma Layer," IEEE Sum. Digest, presented 1968 International Antennas and Propagation Symposium, Boston, Mass. (9-11 September 1968).
5. R. L. Fante, "Mutual Admittances of Infinite Slot Antennas," Proc. IEEE 55, 1754 (October 1967).

UNCLASSIFIED

Security Classification

DOCUMENT CONTROL DATA - R&D		
<small>(Security classification of title, body of abstract and indexing annotation must be entered when the overall report is classified)</small>		
1. ORIGINATING ACTIVITY (Corporate author) The Aerospace Corporation El Segundo, California		2a. REPORT SECURITY CLASSIFICATION Unclassified
		2b. GROUP
3. REPORT TITLE Reentry Plasma Attenuation for S-Band Telemetry Systems		
4. DESCRIPTIVE NOTES (Type of report and inclusive dates)		
5. AUTHOR(S) (Last name, first name, initial) Golden, Kurt E.		
6. REPORT DATE 69 AUG 15	7a. TOTAL NO. OF PAGES 42	7b. NO. OF REFS 4
8a. CONTRACT OR GRANT NO. F04701-69-C-0066	9a. ORIGINATOR'S REPORT NUMBER(S) TR-0066(5220-10)-1 (Formerly TR-0200(4220-10)-3)	
b. PROJECT NO.		
c.	9b. OTHER REPORT NO(S) (Any other numbers that may be assigned this report)	
d.	SAMSO-TR-69-242	
10. AVAILABILITY/LIMITATION NOTICES This document is subject to special export controls and each transmittal to foreign governments or foreign nationals may be made only with prior approval of SAMSO(SMTAE).		
11. SUPPLEMENTARY NOTES		12. SPONSORING MILITARY ACTIVITY Space and Missile Systems Organization Air Force Systems Command U.S. Air Force
13. ABSTRACT The performance of a slot telemetry antenna is analyzed, including the effects of an inhomogeneous plasma sheath on aperture admittance, radiation pattern distortion, antenna window absorption, reflection and absorption losses of the feed network, and total antenna gain. The change in broadside antenna gain induced by the reentry plasma sheath is compared with plane wave signal attenuation calculations. Various antenna matching conditions are evaluated for free-space and reentry-plasma conditions.		

UNCLASSIFIED

Security Classification

14.

KEY WORDS

Slot antenna gain  
Reentry plasma  
Feed network performance  
Antenna matching  
Reentry telemetry antenna

Abstract (Continued)

10. Cont.

The distribution of this report is limited because it contains technology restricted by mutual security acts.

UNCLASSIFIED

Security Classification